PNAS RESEARCH ARTICLE | IMMUNOLOGY AND INFLAMMATION OPEN ACCESS

Intratumoral NKT cell accumulation promotes antitumor immunity in pancreatic cancer

Jiayun Li[a,1], Philip Moresco[a,b,c], and Douglas T. Fearon[a,d,1]

Contributed by Douglas T. Fearon; received February 28, 2024; accepted June 11, 2024; reviewed by Adrian C. Hayday and Weiping Zou

Pancreatic ductal adenocarcinoma (PDA) is a potentially lethal disease lacking effective treatments. Its immunosuppressive tumor microenvironment (TME) allows it to evade host immunosurveillance and limits response to immunotherapy. Here, using the mouse KRT19-deficient (sgKRT19-edited) PDA model, we find that intratumoral accumulation of natural killer T (NKT) cells is required to establish an immunologically active TME. Mechanistically, intratumoral NKT cells facilitate type I interferon (IFN) production to initiate an antitumor adaptive immune response, and orchestrate the intratumoral infiltration of T cells, dendritic cells, natural killer cells, and myeloid-derived suppressor cells. At the molecular level, NKT cells promote the production of type I IFN through the interaction of their CD40L with CD40 on myeloid cells. To evaluate the therapeutic potential of these observations, we find that administration of folinic acid to mice bearing PDA increases NKT cells in the TME and improves their response to anti-PD-1 antibody treatment. In conclusion, NKT cells have an essential role in the immune response to mouse PDA and are potential targets for immunotherapy.

NKT cells | type I IFN | tumor microenvironment | CD40–CD40L interaction | folinic acid

Significance

Our study links the dual requirements for natural killer T (NKT) cells and type I interferon (IFN) signaling in mouse pancreatic ductal adenocarcinoma (PDA). The requirement for type I IFN in the adaptive immune response to solid tumors is fulfilled by NKT cells through their interaction with myelomonocytic cells involving CD40 signaling, a finding consistent with NKT cells phenotypically being at the interface of innate and adaptive immunity.

Secondary to the difficulty of early detection and limited treatment advances, the 5-y survival rate of pancreatic ductal adenocarcinoma (PDA) remains low (1, 2). Immune checkpoint blockade (e.g., anti-PD-1 and anti-CTLA4) has improved the treatment for multiple cancers, but is only effective in a subset of patients with microsatellite-unstable PDA, which comprises less than 5% of all cases (3–5). The lack of tumor-killing T cells and the accumulation of immunosuppressive cells generate an inhibitory tumor microenvironment (TME), which helps PDA evade host immunosurveillance and limits response to immunotherapy (2, 6). Thus, countering the immunosuppressive TME is an important strategy to improve immunotherapy in PDA (7–13).

Type I interferon (IFN) signaling is required for the establishment of robust antitumor adaptive immunity and can enhance the responsiveness to immunotherapy (14, 15). Blocking host type I IFN signaling abrogates the rejection of highly immunogenic tumors (16–19), and induction of type I IFN enhances antitumor immunity in immunoprivileged tumors (13). Interestingly, early but not late, type I IFN signaling is essential for some antitumor immune responses (19). Elucidating the mechanism that contributes to early type I IFN production may contribute to our understanding of how immune-reactive TME forms and lead to the development of new approaches to modulate TME in PDA.

The functions of major immune subsets in the TME of PDA, such as T cells, macrophages, and myeloid-derived suppressor cells (MDSCs), have been objects of study (20–26), but it is critical to characterize the potential roles of the minor immune cell populations. Natural killer T (NKT) cells are a unique subset of T cells that coexpress semi-invariant αβ T cell receptors (TCRs) and NK linage receptors (27–29). More recently, NKT cells have been reported to play important roles in the immunosurveillance of cancer, but their composition and function in PDA are not well understood (30–42).

Different from MHC-restricted T cells, NKT cells can be activated by lipid antigens presented through CD1d on resting dendritic cells (DCs) or directly by cytokines (43–45). Upon activation, NKT cells can up-regulate CD40L and produce cytokines to influence the function of immune subpopulations and therefore orchestrate an effective immune response (46–52). For example, through the engagement of CD40L and CD40, NKT cells facilitate IL-12 production by antigen-presenting cells during activation (47, 48). Also, given that injection of CD40 agonist antibody increases the production of type I IFN stimulated by LPS (53), NKT cells may be able to induce the innate immune cytokine, type I IFN, through their expression of CD40L, perhaps bridging innate and adaptive immunity.

Author affiliations: [a]Cancer Center, Cold Spring Harbor Laboratory, Cold Spring Harbor, NY 11724; [b]Graduate Program in Genetics, Stony Brook University, Stony Brook, NY 11794; [c]Medical Scientist Training Program, Stony Brook University Renaissance School of Medicine, Stony Brook University, Stony Brook, NY 11794; and [d]Meyer Cancer Center, Weill Cornell Medicine, New York, NY 10065

Author contributions: J.L. and D.T.F. designed research; J.L. and P.M. performed research; J.L. analyzed data; and J.L., P.M., and D.T.F. wrote the paper.

Reviewers: A.C.H., King's College London; and W.Z., University of Michigan.

The authors declare no competing interest.

[1]To whom correspondence may be addressed. Email: jiayunli2019@outlook.com or dfearon@cshl.edu.

This article contains supporting information online at https://www.pnas.org/lookup/suppl/doi:10.1073/pnas.2403917121/-/DCSupplemental.

Published July 9, 2024.

Here, we demonstrate that intratumoral NKT cells modulate the TME of mouse PDA, and reveal that the capacity of NKT cells for modulating the TME is mediated by their stimulation of type I IFN production by myeloid cells via CD40 signaling. Additionally, through the administration of folinic acid (FA), we explored the feasibility of increasing the intratumoral accumulation of NKT cells for enhancing the response to immune checkpoint blockade in PDA.

Results

NKT Cells and Immune Control of Mouse PDA. Mouse PDA tumors generated with cancer cells lacking KRT19 expression cannot capture the T cell-excluding chemokine, CXCL12, and are controlled by immune system in a T cell-dependent manner (54). Here, we used this model to evaluate the immune cell populations and signaling pathways required for establishing an immunologically favorable PDA TME. As expected, orthotopic PDA tumors generated with sgKRT19-edited cells were smaller than tumors generated with sgScramble-control cells in wild type C57BL/6 mice (Fig. 1 *A* and *B*). We used flow cytometry and immunofluorescence to compare the composition of immune cells residing within sgKRT19-edited and sgScramble-control orthotopic tumors, respectively (Fig. 1 *C–H* and *SI Appendix*, Figs. S1 and S2 *A–F*). T cells tended to increase in tumors formed with sgKRT19-edited cells (*SI Appendix*, Fig. S2*A*), and significantly T cells had infiltrated into the centers of tumor (Fig. 1*C*). T cells also infiltrated into the centers of the slowly

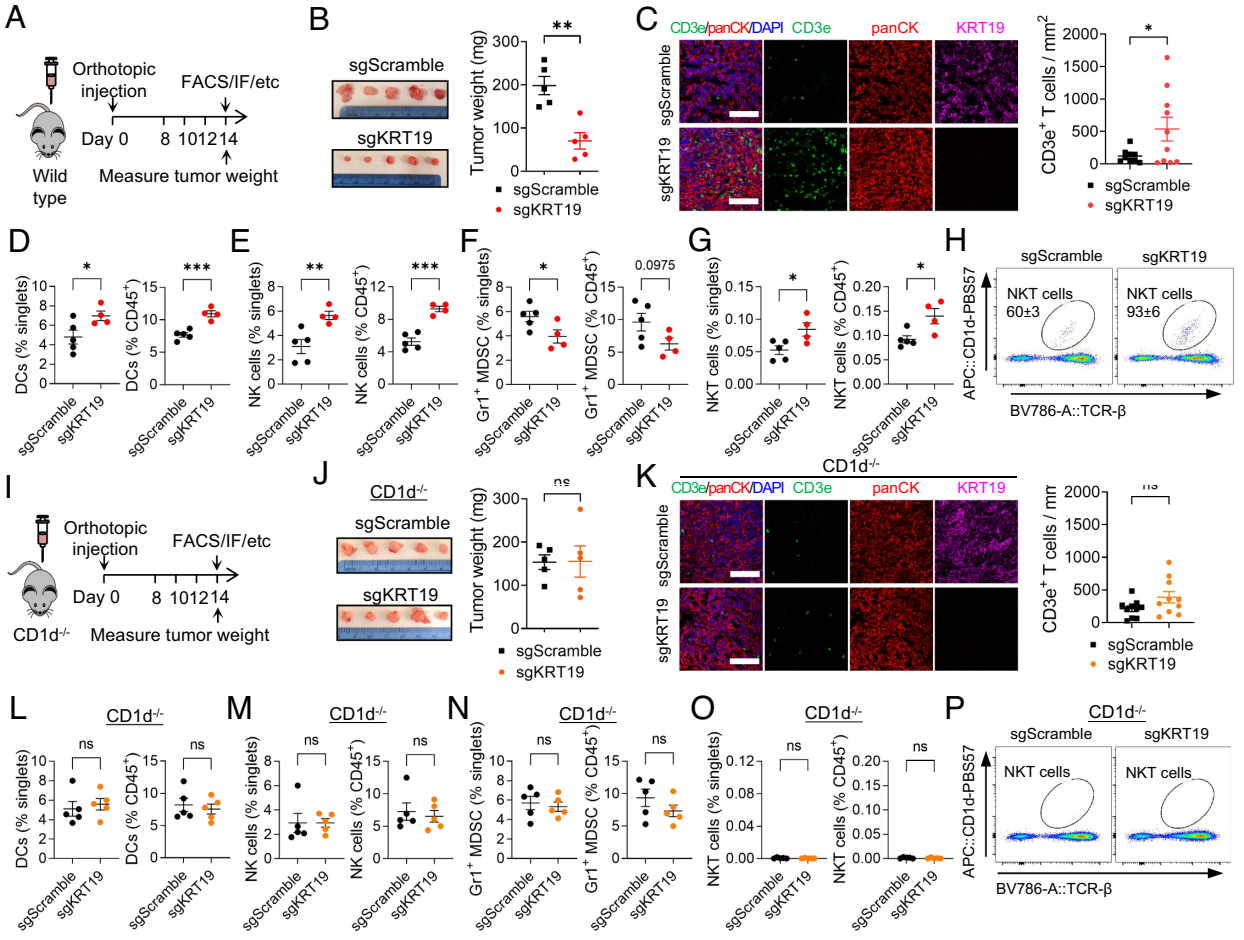

Fig. 1. NKT cells and antitumor immunity in sgKRT19-edited PDA tumors. (*A*) Schematic depicts orthotopic tumor generation with sgKRT19-edited or sgScramble-control KPC1242 mouse PDA cells in wild type mice. (*B*) Weights of orthotopic tumors generated with sgKRT19-edited or sgScramble-control PDA cells were measured on day 14. Mean ± SEM, sgScramble (n = 5) and sgKRT19 (n = 5). Unpaired Student's *t* test, $^{**}P < 0.01$. Data shown are representative of two independent experiments. (*C*) Representative immunofluorescent images show CD3e$^+$ T cells in the center of one sgKRT19-edited and sgScramble-control orthotopic tumor on day 14. (Scale bar, 100 μm.) The number of T cells counted from one image for sgKRT19-edited (n = 10 tumors) and sgScramble-control (n = 9 tumors) orthotopic tumors. Mean ± SEM. Unpaired Student's *t* test, $^{*}P < 0.05$. Data shown are representative of two independent experiments. (*D–G*) The proportions of DCs (*D*), NK cells (*E*), Gr1$^+$ MDSCs (*F*), and NKT cells (*G*) as a percentage of singlets or CD45$^+$ cells from sgKRT19-edited (n = 4) and sgScramble-control (n = 5) orthotopic tumors in wild type mice. Mean ± SEM. Unpaired Student's *t* test, $^{*}P < 0.05$, $^{**}P < 0.01$, $^{***}P < 0.001$. Data shown are representative of two independent experiments. The gating strategy is shown in *SI Appendix*, Fig. S1. (*H*) Representative FACS plots show CD1d–tetramer binding by NKT cells in sgKRT19-edited and sgScramble-control tumors. Data shown are representative of two independent experiments. The gating strategy is shown in *SI Appendix*, Fig. S1. (*I*) Schematic depicts orthotopic tumor generation with sgKRT19-edited and sgScramble-control KPC1242 mouse PDA cells in CD1d$^{-/-}$ mice. (*J*) Weights of orthotopic tumors generated with sgKRT19-edited (n = 5) or sgScramble-control (n = 5) PDA cells in CD1d$^{-/-}$ mice were measured on day 14. Mean ± SEM. Unpaired Student's *t* test, ns = not significant. Data shown are representative of two independent experiments. (*K*) Representative immunofluorescent images show CD3e$^+$ T cells in the center of one sgKRT19-edited and sgScramble-control orthotopic tumor generated in CD1d$^{-/-}$ mice on day 14. (Scale bar, 100 μm.) The number of T cells counted from one image for sgKRT19-edited (n = 10 tumors) and sgScramble-control (n = 10 tumors) orthotopic tumors. Mean ± SEM. Unpaired Student's *t* test, ns = not significant. Data shown are representative of two independent experiments. (*L–O*) The proportions of DCs (*L*), NK cells (*M*), Gr1$^+$ MDSCs (*N*), and NKT cells (*O*) as a percentage of singlets or CD45$^+$ cells isolated from sgKRT19-edited (n = 5) and sgScramble-control (n = 5) orthotopic tumors in CD1d$^{-/-}$ mice were analyzed by flow cytometry. Mean ± SEM. Unpaired Student's *t* test, ns = not significant. Data shown are representative of two independent experiments. The gating strategy is shown in *SI Appendix*, Fig. S1. (*P*) Representative FACS plots show CD1d–tetramer binding NKT cells in sgKRT19-edited and sgScramble-control tumors generated in CD1d$^{-/-}$ mice. Data are representative of two independent experiments. The gating strategy is shown in *SI Appendix*, Fig. S1.

growing sgKRT19-edited subcutaneous (s.c.) tumors but not in sgScramble-control s.c. tumors in which T cells distributed to the invasive margins (*SI Appendix*, Fig. S2 *I* and *J*). NK cells are protective against PDA through cytolytic function (25, 26), whereas accumulation of MDSCs and paucity of DCs in PDA limit antitumor immunity (21, 22). Thus, the observation that more DCs and NK cells but fewer MDSCs accumulated intratumorally as compared to the sgScramble-control tumors (Fig. 1 *D–F*), represents the immune-activated phenotype of sgKRT19-edited PDA tumors. Notably, NKT cells were enriched in sgKRT19-edited tumors, showing increased numbers and percentages of both total single cells and $CD45^+$ cells (Fig. 1 *G* and *H*).

We evaluated the potential role for NKT cells in PDA tumor immunosurveillance by comparing sgKRT19-edited and sgScramble-control tumors generated in $CD1d^{-/-}$ mice that lack of NKT cells (Fig. 1 *I–P*). In contrast to tumors formed in wild type mice (Fig. 1*B*), sgKRT19-edited orthotopic tumors in $CD1d^{-/-}$ mice were equivalent in size to sgScramble-control tumors (Fig. 1*J*). Also, the numbers of $CD3e^+$ T cells infiltrating the centers of sgKRT19-edited tumors were low and similar to those in sgScramble-control tumors (Fig. 1*K*). The numbers of other intratumoral immune cells were similar in the sgKRT19-edited and sgScramble-control orthotopic PDA tumors in $CD1d^{-/-}$ mice (Fig. 1 *L–P* and *SI Appendix*, Fig. S3 *A–F*). Also, the s.c. tumors formed in $CD1d^{-/-}$ mice with sgKRT19-edited and sgScramble-control cells had similar growth rates (*SI Appendix*, Fig. S3 *G* and *H*) and few T cells infiltrating to the centers (*SI Appendix*, Fig. S3*I*). Together, these data demonstrate that NKT cells are required for the formation of an immune-reactive TME and the tumor-restraining adaptive immune response of sgKRT19-edited PDA tumors.

Early Type I IFN Signaling and Adaptive Immune Control of PDA. We evaluated the immune signaling pathways that might mediate the dependency on NKT cells in the immune control of sgKRT19-edited tumors. Gene set enrichment analysis (GSEA) of bulk RNA-sequencing data (54) of s.c. PDA tumors showed that the types I and II IFN responses were among the top up-regulated pathways (Fig. 2 *A* and *B*). While the upregulation of IFN gamma response most likely reflected adaptive immune responses in the sgKRT19-edited PDA tumors, the upregulation of the IFN alpha pathway suggested that an innate immune response was also occurring. Since NKT cells are at the interface of innate and adaptive immunity, we assessed whether the type I IFN pathway depended on the presence of these cells. With sgKRT19-edited and sgScramble-control PDA s.c. tumors inoculated into wild type mice and $CD1d^{-/-}$ mice, we compared the expression of IFN-β and the interferon-stimulated genes (ISGs). The increased transcription of IFN-β and ISGs in sgKRT19-edited tumors compared to sgScramble-control tumors that occurred in wild type mice was absent in $CD1d^{-/-}$ mice lacking NKT cells (Fig. 2*C*). These findings indicate that NKT cells have a role in generating type I IFN in the sgKRT19-edited PDA tumors.

We assessed whether type I IFN response was related to the requirement for NKT cells to mediate an adaptive immune response by inoculating sgKRT19-edited and sgScramble-control PDA cells into IFN-alpha receptor I knockout ($IFNARI^{-/-}$) mice (Fig. 3*A*). In contrast to the smaller tumor sizes of the sgKRT19-edited PDA tumors relative to the sgScramble-control PDA tumors in wild type mice (Fig. 3*B* and *SI Appendix*, Fig. S4 *A* and *B*), the sizes of both types of tumors were similar in $IFNARI^{-/-}$ mice in orthotopic and s.c. models (Fig. 3*C* and *SI Appendix*, Fig. S4 *C* and *D*). Thus, type I IFN signaling is required for the immune control of sgKRT19-edited tumors. The enhanced accumulation of NKT cells and NK cells was maintained in sgKRT19-edited PDA tumors growing in the $IFNARI^{-/-}$ mice (Fig. 3 *D* and *E* and *SI Appendix*, Fig. S4 *E–J*), suggesting that their intratumoral presence does not depend on type I IFN signaling. In contrast, the differences in infiltrating T cells, DCs, and MDSCs

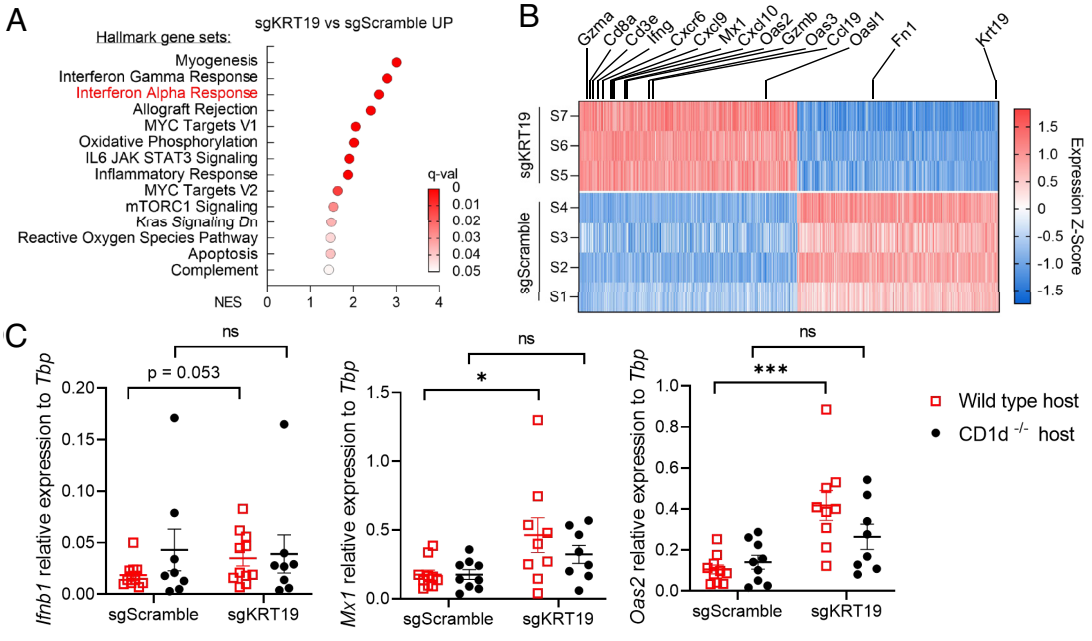

Fig. 2. NKT cells and type I IFN in sgKRT19-edited tumors. (*A*) GSEA of RNAseq data from sgKRT19-edited (n = 3) and sgScramble-control (n = 4) s.c. tumors show pathways that are significantly up-regulated in sgKRT19-edited tumors. (*B*) Heat map shows normalized expression z-scores of the most differentially expressed genes by RNAseq analysis of sgKRT19-edited (n = 3) tumors compared to sgScramble control (n = 4) s.c. tumors. Published RNAseq data (54) was used for the analysis in (*A*) and (*B*). (*C*) qPCR measurements are shown of type I IFN-related gene expression relative to *Tbp* in sgKRT19-edited and sgScramble-control s.c. tumors generated in wild type mice (red open square) and $CD1d^{-/-}$ mice (black solid circle). Mean ± SEM, sgScramble in wild type (n = 10), sgKRT19 in wild type (n = 9), sgScramble in $CD1d^{-/-}$ (n = 9), and sgKRT19 in $CD1d^{-/-}$ (n = 8). Unpaired Student's *t* test, ns = not significant, $*P < 0.05$, $***P < 0.001$. Data shown are representative of two independent experiments.

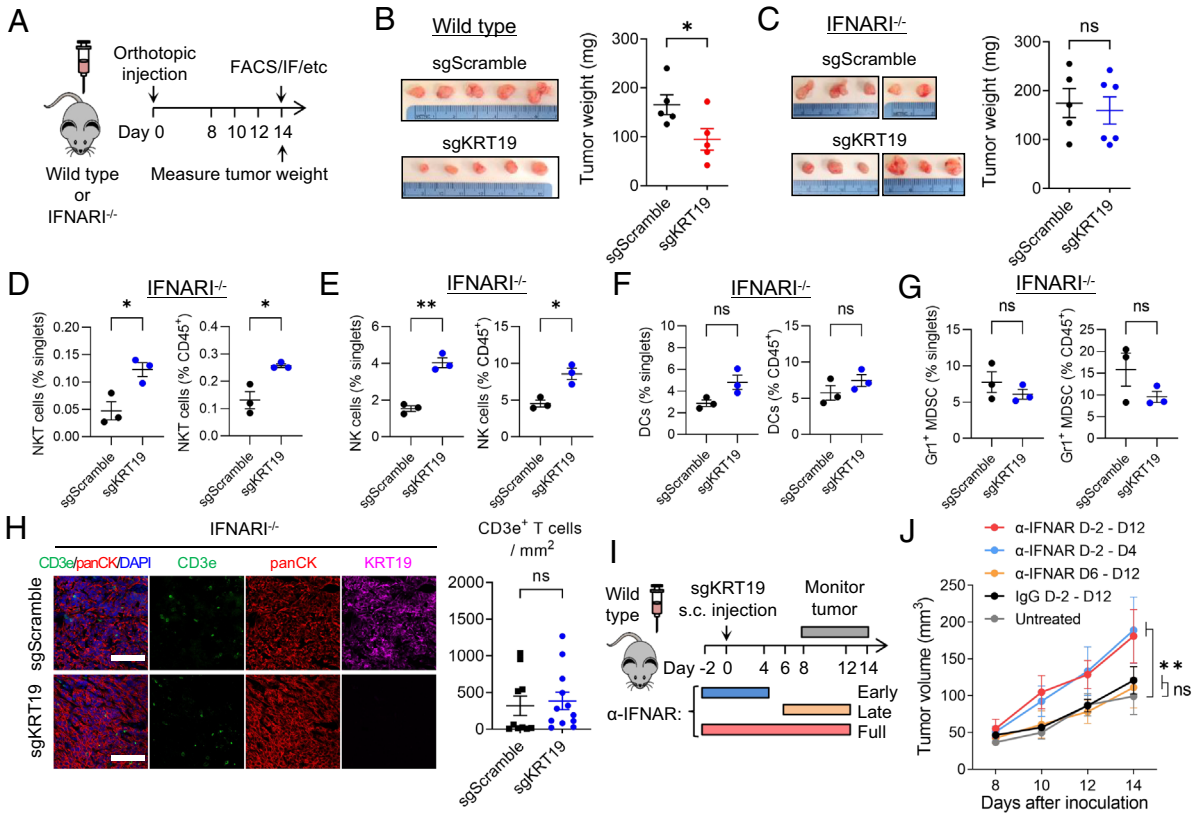

Fig. 3. Type I IFN and immune control of sgKRT19-edited PDA tumors. (*A*) Schematic depicts orthotopic tumor generation with sgKRT19-edited or sgScramble-control KPC1242 mouse PDA cells in wild type or IFNARI$^{-/-}$ mice. (*B* and *C*) Weights of orthotopic tumors generated with sgKRT19-edited or sgScramble-control PDA cells in wild type (*B*) or IFNARI$^{-/-}$ (*C*) mice were measured on day 14. Mean ± SEM, sgScramble-control in wild type (n = 5), sgKRT19-edited in wild type (n = 5), sgScramble-control in IFNARI$^{-/-}$ (n = 5), and sgKRT19-edited in IFNARI$^{-/-}$ (n = 6). Unpaired Student's *t* test, ns = not significant, *$P < 0.05$. Data shown are representative of two independent experiments. (*D*–*G*) The proportions of NKT cells (*D*), NK cells (*E*), DCs (*F*), and Gr1$^+$ MDSCs (*G*) as a percentage of singlets or CD45$^+$ cells from sgKRT19-edited (n = 3) and sgScramble-control (n = 3) orthotopic tumors in IFNARI$^{-/-}$ mice were analyzed by flow cytometry. Mean ± SEM. Unpaired Student's *t* test, ns = not significant, *$P < 0.05$, **$P < 0.01$. The gating strategy is shown in *SI Appendix*, Fig. S1. Data shown are representative of two independent experiments. (*H*) Representative immunofluorescent images show CD3e$^+$ T cells in the center of one sgKRT19-edited and sgScramble-control orthotopic tumor generated in IFNARI$^{-/-}$ mice on day 14. (Scale bar, 100 μm.) The number of T cells counted in one image of each tumor is shown for sgKRT19-edited (n = 12) and sgScramble-control (n = 10) orthotopic tumors. (Scale bar, 100 μm.) Mean ± SEM. Unpaired Student's *t* test, ns = not significant. Data shown are representative of two independent experiments. (*I*) Schematic depicts anti-IFNAR antibody blocking experiments. sgKRT19-edited PDA cells were s.c. injected into wild type mice, and IFNAR blocking antibody or isotype control IgG were injected every other day from day -2 through day 12, from day -2 through day 4, or from day 6 through day 12. (*J*) Volumes are shown of sgKRT19-edited s.c. tumors with treatments as indicated in (*I*). Mean ± SEM, n = 5 each group. Row-mean one-way ANOVA followed by multiple comparison compared to the untreated group, ns = not significant, **$P < 0.01$.

between sgKRT19-edited and sgScramble-control orthotopic PDA tumors were attenuated when generated in the IFNARI$^{-/-}$ mice (Fig. 3 *F*–*H* and *SI Appendix*, Fig. S4*K*). Therefore, the functions of NKT cells are upstream of type I IFN and, possibly, the adaptive immune response in sgKRT19-edited tumors.

To specify the time at which the innate immune role of type I IFN signaling is required, we administered anti-IFNAR neutralizing antibody to wild type mice bearing sgKRT19-edited s.c. PDA tumors to block type I IFN signaling on different days during tumor development (Fig. 3 *I* and *J*). Administering anti-IFNAR antibody starting 6 d after tumor inoculation did not alter the growth rate of the sgKRT19-edited tumors. However, when the anti-IFNAR antibody administration was initiated before tumor inoculation from day -2 through day 4, the tumor growth rates were more rapid and were similar to continuous neutralization of IFNAR signaling. Thus, type I IFN is providing an innate immune signal that is required for the subsequent antitumor adaptive immune response.

CD40 Signaling, NKT Cells, and Type I IFN. To identify the cell types producing type I IFN in sgKRT19-edited PDA tumors, we focused on intratumoral CD11c$^+$ and CD11b$^+$ cells, as these cells have been reported to be type I IFN-producing cells in other cancers (55, 56). With RNA fluorescence in situ hybridization (RNA-FISH) and probes specific for *Itgax* (encoding CD11c), *Itgam* (encoding CD11b), and *Ifnb1*, we found that in sgKRT19-edited PDA tumors, *Ifnb1* mRNA was present predominantly in cells that expressed either CD11b and/or CD11c (~94%) (Fig. 4*A* and *SI Appendix*, Fig. S5). Also, among the IFN-β producing cells, CD11b$^+$CD11c$^+$ cells were the most abundant (~42%). Accordingly, we conclude that myeloid cells are the major source of type I IFN in sgKRT19-edited PDA tumors.

Reminiscent of the report that treating mice with anti-CD40 agonistic antibody enhances LPS-induced type I IFN synthesis (53), more than 80% of the *Ifnb1*$^+$ cells in sgKRT19-edited tumors coexpressed CD40 (Fig. 4*B*). When we administered neutralizing anti-CD40L antibody to mice bearing s.c. PDA tumors, there was reduced expression of ISGs in both sgKRT19-edited and sgScramble-control PDA tumors as compared to tumors in IgG control antibody-treated mice (Fig. 4*C*). In addition, a single treatment with agonistic anti-CD40 antibody enhanced type I IFN production in unmodified parental KPC1242 s.c. PDA tumors expressing KRT19 and led to control of tumor growth (*SI Appendix*, Fig. S6 *A*–*D*). By RNA-FISH, the CD11b/CD11c positive subpopulation of myeloid cells was demonstrated to have *Ifnb1* transcripts in the agonistic anti-CD40 antibody-treated tumors (*SI Appendix*, Fig. S6 *E* and *F*). Thus, regulation of type I

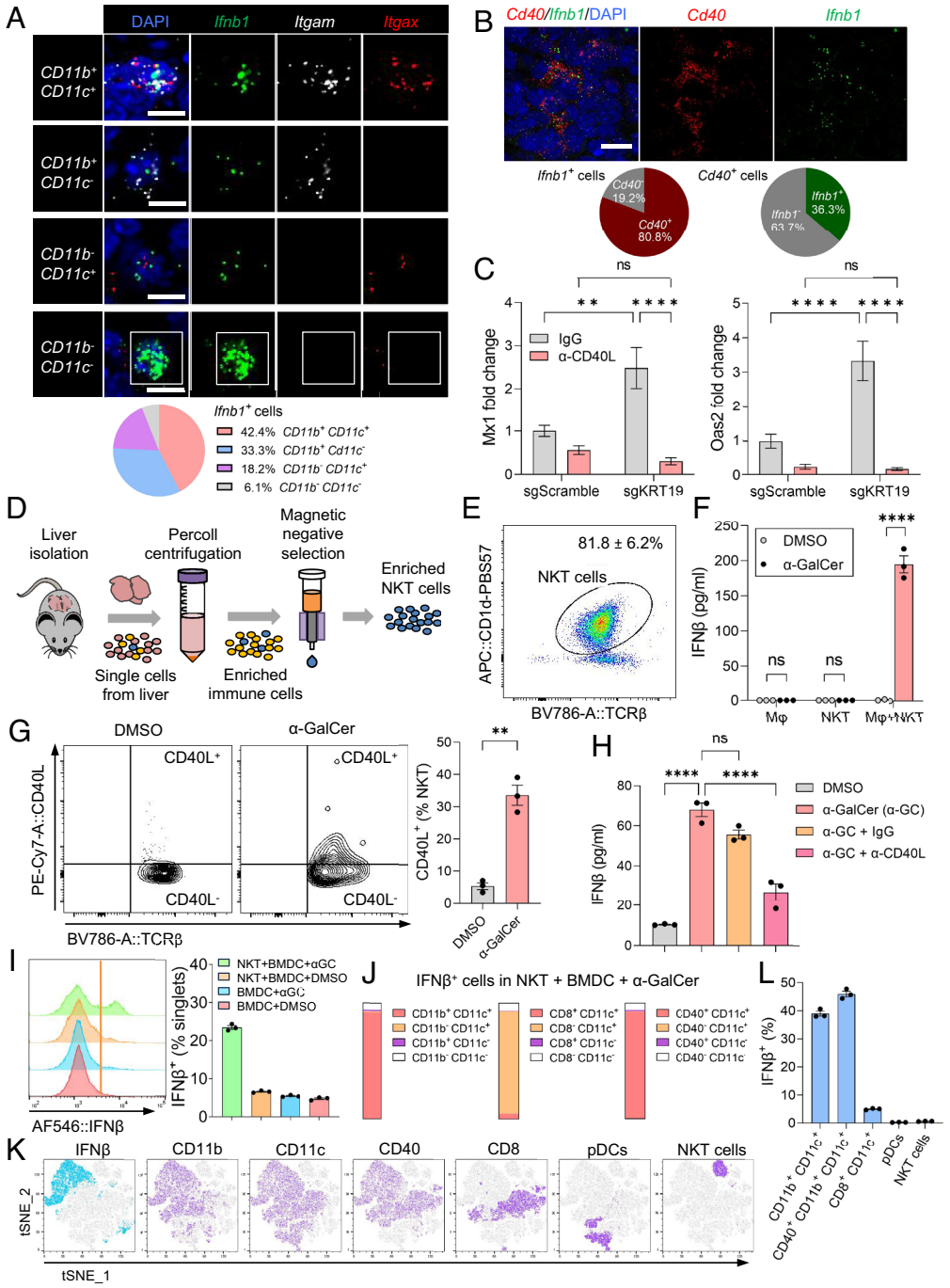

Fig. 4. NKT cells, type I IFN production and CD40–CD40L signaling. (*A*) Representative RNA FISH image is shown of Ifnb1, Itgam, and Itgax expression in sgKRT19-edited s.c. tumors in wild type mice. (Scale bar, 10 μm.) Percentage shows Ifnb1-expressing cells defined by coexpression with Itgam or Itgax. (*B*) Representative RNA FISH image is shown of Ifnb1 and Cd40 coexpression in sgKRT19-edited s.c. tumors from wild type mice. (Scale bar, 20 μm.) Percentage shows Ifnb1-expressing cells defined by coexpression with Cd40, and of Cd40-expressing cells defined by coexpression with Ifnb1 in sgKRT19-edited tumors. Data shown are representative of two independent experiments. (*C*) qPCR measurements are shown of type I IFN-related gene expression in sgKRT19-edited or sgScramble-control s.c. tumors from wild type mice, treated with isotype control IgG or anti-CD40L antibody. Mean ± SEM, sgScramble-control + IgG (n = 6), sgScramble-control + anti-CD40L (n = 7), sgKRT19-edited + IgG (n = 7) and sgKRT19-edited + anti-CD40L (n = 8). Two-way ANOVA followed by multiple comparison. ns = not significant, $^{**}P < 0.01$, $^{****}P < 0.0001$. Data shown are representative of two independent experiments. (*D*) Schematic depicts mouse NKT cell isolation from livers by negative selection using magnetic beads bearing antibodies to CD8, CD19, CD11b, CD11c, Gr1, TCRγδ, CD24, Ter-119, CD49b, and CD62L. (*E*) Flow cytometry characterization is shown of isolated NKT cells stained with antibody to TCR-beta and CD1d–tetramers. The gating strategy is shown in *SI Appendix*, Fig. S7*B*. Percentage was calculated in singlets. Data shown are representative of two independent experiments. (*F*) ELISA quantification is shown of IFNβ in the culture supernatants from NKT cells and peritoneal macrophages cultured alone or together, with or without stimulation by α-GalCer for 48 h. Mean ± SEM, n = 3. Two-way ANOVA followed by multiple comparison, ns = not significant, $^{****}P < 0.0001$. Data are representative of three independent experiments. (*G*) Flow cytometry analysis shows CD40L expression by NKT cells treated with or without α-GalCer. Mean ± SEM, n = 3. Unpaired Student *t* test, $^{**}P < 0.01$. (*H*) ELISA quantification is shown of IFNβ in the supernatants from NKT cells and peritoneal macrophages cocultured for 48 h with DMSO or α-GalCer, and in the absence or presence of isotype control IgG or anti-CD40L antibody. One-way ANOVA followed by multiple comparison. ns = not significant, $^{****}P < 0.0001$. Data shown are representative of two independent experiments. (*I*) The proportions of IFNβ-producing cells in cocultures of NKT cells and BMDCs were determined by flow cytometry analysis. Cells were cultured for 48 h with DMSO or α-GalCer followed by 12 h of BFA treatment. Mean ± SEM, n = 3. The gating strategy is shown in *SI Appendix*, Fig. S8. Data shown are representative of two independent experiments. (*J*) IFNβ-producing cells in coculture of NKT cells and BMDCs treated with α-GalCer followed by BFA were characterized by their costaining of CD11c, CD11b, CD40, and CD8. Mean of n = 3 is shown. The gating strategy is shown in *SI Appendix*, Fig. S8. Data shown are representative of two independent experiments. (*K*) tSNE plots show cell populations defined by the staining of IFNβ, CD11b, CD11c, CD40, CD8, pDC, and NKT cells in single cells as gated in *SI Appendix*, Fig. S8. tSNE_1 and tSNE_2 were generated by FlowJo in a representative coculture of NKT cells and BMDCs treated with α-GalCer followed by BFA. (*L*) The proportions of IFNβ-producing cells in subpopulations from the coculture of NKT cells and BMDCs treated with α-GalCer followed by BFA were characterized by flow cytometry. Mean ± SEM, n = 3. The gating strategy is shown in *SI Appendix*, Fig. S8. Data shown are representative of two independent experiments.

IFN production by CD40 signaling may also occur in PDA tumors composed of unmodified cancer cells.

Based on the findings that intratumoral type I IFN is downregulated in CD1d$^{-/-}$ mice lacking NKT cells (Fig. 2*C*), that intratumoral accumulation of NKT cells is independent of type I IFN (Fig. 3*D*), that NKT cells express CD40L at the initiation of immune response (45), and that myeloid cells are the intratumoral source of type I IFN (Fig. 4*A*), we hypothesized that NKT cells may stimulate production of type I IFN through interaction of their CD40L with CD40 expressed by myeloid cells. To test this hypothesis, NKT cells were purified from mouse livers (Fig. 4 *D* and *E* and *SI Appendix*, Fig. S7 *A* and *B*), cocultured with peritoneal macrophages, and activated with α-galactosylceramide (αGalCer) (47, 57). After 48 h, IFN-β was detected in the supernatants in cocultures of α-GalCer-stimulated NKT cells and macrophages, but not in cultures of NKT cells or macrophages alone, or in unstimulated cocultures (Fig. 4*F*).

As expected, RNA-FISH showed that macrophages, but not NKT cells, produced type I IFN (*SI Appendix*, Fig. S7*C*). α-GalCer-stimulated NKT cells increased their surface-expression of CD40L (Fig. 4*G* and *SI Appendix*, Fig. S7*D*), and blocking the CD40–CD40L interaction with anti-CD40L antibody inhibited IFNβ production by the cocultured cells (Fig. 4*H*). Furthermore, we characterized IFNβ-producing cells in cocultured NKT cells and bone marrow–derived DCs (BMDCs) by flow cytometry analysis (Fig. 4 *I–L* and *SI Appendix*, Fig. S8). IFNβ-preducing cells were induced in the cocultures treated with α-GalCer (Fig. 4*I*), and were mainly $CD11b^+/CD11c^+/CD40^+/CD8^-$ (Fig. 4 *J* and *K*). In contrast to $CD11b^+CD11c^+CD40^+$ cells, $CD11c^+CD8^+$ cells, plasmacytoid DCs (pDCs), or NKT cells did not produce IFNβ in the cocultures stimulated with α-GalCer (Fig. 4*L*). Thus, NKT cells regulate type I IFN production in vitro by myelomonocytic cells through their expression of CD40L upon activation.

FA, NKT Cells, and the Response of Mouse PDA to Anti-PD-1 Antibody. FA, also known as leucovorin, has been reported to induce NKT cell accumulation in the intestines of neonatal mice (58). Accordingly, when we treated mice bearing unmodified parental KPC1242 s.c. PDA tumors with oral administered FA, we observed a dose-dependent increase of NKT cells in tumors (Fig. 5 *A* and *B*). We identified multiple immune response pathways that were up-regulated in the FA-treated group as compared with the control group of mice (Fig. 5*C*). Notably, type I IFN signaling was up-regulated in FA-treated KPC1242 s.c. PDA tumors concomitantly with the increased accumulation of NKT cells (Fig. 5*C*).

Since the tumors treated with FA recapitulated the immune-reactive TME of sgKRT19-edited tumors, and the latter tumors respond to anti-PD-1 antibody (54), we assessed whether treatment with FA-induced sensitivity of unmodified parental KPC1242 s.c. PDA tumors to anti-PD-1 antibody immunotherapy (Fig. 5*D*). Administration of FA or anti-PD-1 antibody alone did not affect tumor growth rate, but the combination resulted in a twofold reduction of tumor growth rate that occurred in more than half of the treated mice (Fig. 5 *E–G* and *SI Appendix*, Fig. S9*A*). Moreover, the synergy between FA and anti-PD-1 antibody requires NKT cells and type I IFN signaling, as the suppression of tumor growth was not observed in $CD1d^{-/-}$ or $IFNARI^{-/-}$ mice (Fig. 5 *H* and *I* and *SI Appendix*, Fig. S9 *B–E*). These findings suggest that FA may be a candidate for enhancing immune checkpoint blockade in PDA.

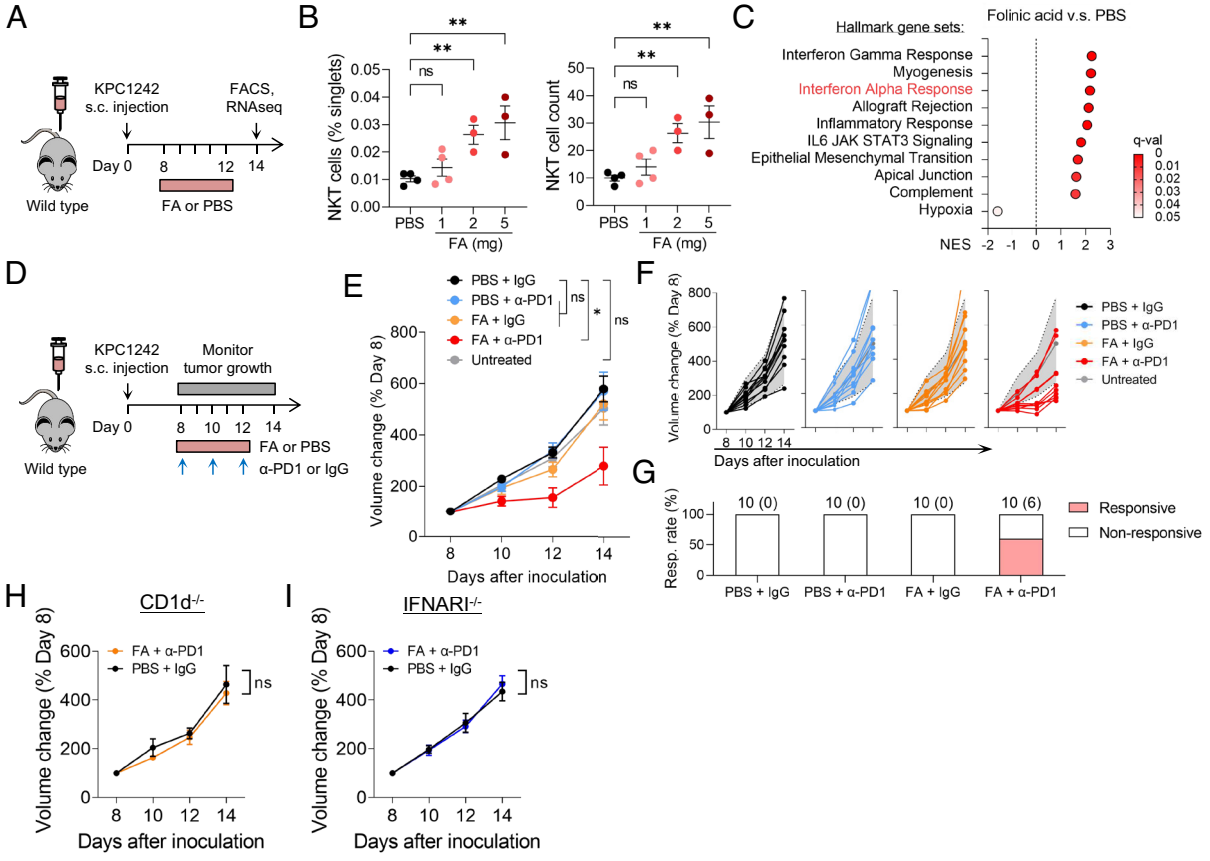

Fig. 5. FA, NKT cell accumulation, and sensitization of mouse PDA tumors to treatment with anti-PD-1 antibody. (*A*) Schematic depicts FA treatment of s.c. tumors generated with parental KPC1242 mouse PDA cells in wild type mice. FA or PBS were administered by oral gavage daily from days 8 through 12 after tumor inoculation. (*B*) Flow cytometry measurements of infiltrating NKT cells as percentages of singlets or $CD45^+$ cells isolated from s.c. tumors treated with different doses of FA or PBS. Mean ± SEM PBS (n = 4), 1 mg FA (n = 4), 2 mg FA (n = 3), and 5 mg FA (n = 3). One-way ANOVA followed by multiple comparison. ns = not significant, $*P < 0.05$, $**P < 0.01$. The gating strategy is shown in *SI Appendix*, Fig. S1*A*. (*C*) GSEA shows RNA from PBS- or FA-treated (2 mg) tumors. Three tumors from each group of mice were used for RNAseq. (*D*) Schematic depicts FA and anti-PD-1 antibody combination treatment in s.c. KPC1242 PDA tumors. 2 mg FA were administered daily, and isotype control IgG or anti-PD-1 antibody was administered every other day from days 8 to 12 after tumor inoculation. (*E*) Volume change is shown of s.c. tumors treated with FA (2 mg) and anti-PD-1 antibody (200 μg) alone or in combination. Mean ± SEM, n = 5 each group. Row-mean one-way ANOVA followed by multiple comparison to the PBS + IgG control group, ns = not significant, $*P < 0.05$. Data shown are representative of two independent experiments. (*F*) Individual volume change is shown of s.c. tumors treated with FA and anti-PD-1 antibody alone or in combination. The gray area shows the range ± SEM of untreated tumors, n = 10 each group. Data shown are representative of two independent experiments. (*G*) Response rate of s.c. tumors to the indicated treatment. Tumors with growth rate slower than untreated tumors (underneath gray area) in (*F*) are considered as responsive. Data shown are representative of two independent experiments. (*H* and *I*) Volume changes are shown of s.c. tumors treated with PBS + IgG control or FA + anti-PD-1 antibody in $CD1d^{-/-}$ mice (*H*) or $IFNARI^{-/-}$ mice (*I*). Mean ± SEM n = 5 each group. Simple linear regression and slopes comparison, ns = not significant. Data are representative of two independent experiments.

Discussion

Our study demonstrates the essential role of NKT cells in establishing an antitumor immune TME in PDA by facilitating the biosynthesis of the innate immune cytokine, type I IFN, to initiate the adaptive antitumor immune response (*SI Appendix*, Fig. S10). This observation emphasizes the role of NKT cells in bridging innate and adaptive immunity and is consistent with their characteristic expression of markers of both NK cells and T cells. A previous study has noted that NKT cells suppress intraepithelial neoplasia (PanIN) lesions (precancerous stage of PDA) growth by rewiring tumor-associated macrophages (59). Activation of NKT cells has been utilized as an immunotherapeutic strategy against mouse PDA (60, 61). Here, by analyzing the regulation of type I IFN production in sgKRT19-edited PDA tumors lacking T cell-excluding CXCL12-coat, we revealed that CD40L on NKT cells interacts with CD40 on myeloid cells to enhance type I IFN production, thereby achieving the requirement for this innate immune cytokine to modulate adaptive immunity in PDA. This observation provides a mechanistic basis for facilitating the function of NKT cells in therapy of PDA.

Type I IFN can impact the immunological effects of multiple immune cells including cross-presenting DCs, T cells, NK cells, and MDSCs (62–66). Particularly, type I IFN facilitates the recruitment of T cells through the induction of CXCL10 (67–69). Indeed, the infiltration of T cells into the center of PDA tumors was attenuated in both CD1d$^{-/-}$ and IFNARI$^{-/-}$ mice (Figs. 1*K* and 3*H*). Thus, regulating the production of type I IFN, is a way that NKT cells can affect the intratumoral infiltration of T cells, and potentially impact the sensitivity of tumors to immunotherapy. In parallel with this role of NKT cells in the mouse model of PDA, type I IFN signaling pathway was observed down-regulated in a model of prostate cancer in Jα18$^{-/-}$ mice that lack invariant NKT cells (40). Thus, the regulation of type I IFN by NKT cells is possibly a general pattern in tumor immunosurveillance.

More recently, CD1d has been found to influence the intrinsic function of macrophages on lipid metabolism and NLRP3 inflammasome-stimulated cytokine production (70, 71). In contrast to our study of the absence of type I IFN in PDA-bearing CD1d-deficient mice, CD1d-deficient macrophages secrete more IFN-β and proinflammatory cytokines upon TLR stimulation (70). This circumstance may be related to the high individual variation of *Ifnb1* occurring in both sgKRT19-edited and sgScramble-control PDA tumors in CD1d$^{-/-}$ mice (Fig. 2*C*). However, the role of CD1d on macrophages is unlikely to be related to the essential role of NK T cells in the production of intratumoral type I IFN and the subsequent adaptive immune response.

Activation of NKT cells with α-GalCer or adoptive transfer of modified NKT cells is often used in NKT cell-based therapies (60, 61, 72–76). Our study explored another way to harness NKT cells for immunotherapy by showing that treatment with FA of PDA-bearing mice increases intratumoral accumulation of NKT cells and can promote efficacy of T cell checkpoint immunotherapy. In support of this possibility, chemotherapy regimens containing FA have been shown to improve clinical response to treatment with anti-PD-1 antibody (77, 78).

Materials and Methods

Animals. Experiments were done with 8- to 12-wk-old, age-matched male mice. C57BL/6J (#000664), IFNARI$^{-/-}$ [B6(Cg)-*Ifnar1*$^{tm1.2Ees}$/J, #028288], and CD1d$^{-/-}$ [B6.129S6-Del(3Cd1d2-Cd1d1)1Sbp/J, #008881] mice were purchased from Jackson Laboratory. All mice were housed in a specific pathogen-free facility at Cold Spring Harbor Laboratory (CSHL), on a 12 h light/dark cycle. To avoid the impact of stress during transfer, newly purchased mice were housed in the onsite facility for at least 2 wk before conducting experiments. Wildtype mice with matching age and sex were included in parallel with CD1d$^{-/-}$ or IFNAR1$^{-/-}$ mice as control for the comparison between sgKRT19-edited and sgScramble-control tumors. FA dosage experiment has been done once, and all other in vivo experiments have been done at least twice, and the representative data are shown. All animal experiments were approved by the CSHL Institutional Animal Care and Use Committee (IACUC) in concordance with the NIH "Guide for the Care and Use of Laboratory Animals."

Cell Lines. The mouse PDA cell line, KPC1242, was a gift from Dr. David Tuveson at Cold Spring Harbor Laboratory and maintained in our lab. sgScramble-edited and sgKRT19-edited KPC1242 cell lines were generated in our lab previously (54). All mouse PDA cell lines were cultured at 37 °C and 5% CO_2 in DMEM (Corning, 10-013-CV) supplemented with 10% FBS (Seradigm, 1500-500), 100 units/mL penicillin, and 100 μg/mL streptomycin.

Tumor Models.

s.c. model. To generate s.c. tumors, 2.5 × 10^5 cells in PBS were injected into the right flank of mice after shaving. Tumor length (L) and width (W) were measured with digital caliper every 2 or 3 d and calculated according to the following formula: $V = (L \times W^2)/2$.

Orthotopic model. To generate orthotopic tumors, 1 × 10^4 cells in a 50/50 PBS/Matrigel (Corning, growth factor reduced, 356231) mixture were injected to the pancreas of mice. Tumor mass was measured at the experimental endpoint.

In detail, mice were shaved the day before orthotopic injection. On the day of injection, Single cell suspensions of sgKRT19-edited or sgScramble-control cancer cells were prepared in 50/50 PBS/Matrigel (Corning, growth factor reduced, 356231). After opening a small incision on the left side of the mice below the chest, the spleen was pulled out carefully with tweezers to bring out the pancreas. 1 × 10^4 cells were injected to the tail of pancreas in 5 μL volume for each mouse with a gastight syringe and 32-gauge needle (Hamilton, 25 μL Gastight Syringe Model 1702). To avoid wound tumor formation, after withdrawing cells, the needle was wiped with ethanol wipes to kill cells attached to the outside of the needle before injection. The formation of a small transparent bump on the pancreas indicated a successful injection. If no bump was observed, the injection probably leaked and would result in a wound tumor, so the mouse would be killed immediately. After injection, the needle was held in the pancreas for about 30 s for Matrigel to solidify as a prevention of leakage, and the needle entry point was cauterized to prevent bleeding and kill any back flashed cancer cells to prevent wound tumor formation. After a successful injection, the pancreas and spleen were gently pulled back into the abdominal cavity, the muscle layer was sutured with biodegradable sutures (Ethicon, 5-0 Coated VICRYL VIOLET 1X18" P-3, J463G), and skin was closed with clips (ROBOZ, Reflex 7 mm Wound Clips, RS-9258). Triple antibiotic ointment was applied to the skin wound to prevent infection. Mice that underwent surgery were monitored in a heating chamber until recovery before returning to the nest. The well-being of mice was checked in the following 2 d. If any adverse appearance was observed, the mice would be euthanized according to the regulations by IACUC at CSHL. Seven days after the injection, clips were removed. Orthotopic tumors were isolated 14 d after injection for an endpoint comparison. Tumors formed from leakage were excluded. Images of tumor were captured, and weights were measured on a scale. One piece of tumor was cut with a blade and put in O.C.T. compound (SAKURA, Tissue-Tek O.C.T. Compound, 4583), frozen on dry ice in a model, and kept at −80 °C until cutting slides for imaging. The rest of the tumor was digested for FACS analysis of immune cell composition as described in "Flow Cytometry."

Antibody Treatments.

Anti-PD1 treatment. Tumor-bearing mice received three intraperitoneal (i.p.) injections of 200 μg of anti-mouse PD-1 antibody (BioXcell, BE0273, clone 29F.1A12) or rat IgG2a isotype control (BioXcell, BE0089, clone 2A3), every other day from days 8 to 12 posttumor inoculation.

Anti-IFNaRI blockade. Mice were i.p. injected with 500 μg of anti-mouse IFNaR-1 antibody (BioXcell, BE0241, clone MAR1-5A3) or mouse IgG1 isotype control (BioXcell, BE0083, clone MOPC-21), every other day, from 2 d prior to tumor inoculation to 12 d postinoculation, from 2 d prior to tumor inoculation to 4 d postinoculation, or from 6 d prior to tumor inoculation to 12 d postinoculation.

Anti-CD40L blockade. Mice were i.p. injected with 500 μg of anti-mouse CD40L (CD154) antibody (BioXcell, BE0017-1, clone MR-1) or polyclonal Armenian

hamster IgG control (BioXcell, BE0091), every other day, from 2 d prior to tumor inoculation to 12 d postinoculation.

Anti-CD40 activation. Mice were i.p. injected with 200 μg of anti-mouse CD40 antibody (BioXcell, BE0016-2, clone FGK4.5) or rat IgG2a isotype control (BioXcell, BE0089, clone 2A3) once on day 11 after tumor inoculation.

FA Treatments. 1 mg, 2 mg, or 5 mg of FA (Sigma, PHR1541) in 100 μL PBS or PBS along was administrated by oral gavage daily from day 8 to day 12 after tumor inoculation. FA did not fully dissolve in PBS at above concentrations, and the suspensions were given to mice.

Immunofluorescence. Fresh frozen tumors embedded in Tissue-Tek OCT (Sakura, 4583) were sectioned at 10 μm on a Cryostat-Leica CM 3050S. For immunofluorescent (IF) staining, tumor slices were fixed with PLP buffer (1% PFA, 2 mg/mL $NaIO_4$, 14 mg/mL L-lysine in phosphate buffer) at room temperature (RT) for 5 to 10 min. After three brief washes with PBS, a hydrophobic barrier was drawn around the tumor slice with the ImmEdge PAP pen (Vector Laboratories, H-4000) and left to air dry for 3 min. The slices were then permeabilized and blocked with IF wash buffer (0.1% BSA, 0.2% Triton X-100, 0.05% Tween-20, 0.05% NaN_3 in PBS) containing 10% normal goat serum (Thermo, 16210064) at RT for 1 h. After the blocking, the tumor slices were stained at 4 °C overnight with fluorochrome-conjugated antibodies including: AF488-anti-CD3 (BioLegend, 100210), AF568-anti-KRT19 (Abcam, ab203445), AF594-anti-KRT19 (Abcam, ab203443), and AF647-anti-panCK (NOVUS, NBP1-48348AF647). After, the slices were washed with IF wash buffer three times, for 2 min each. Nuclei were counterstained with DAPI (Thermo, R37606) at room temperature for 5 min. After the staining, the slices were mounted with ProLong Glass Antifade Mountant (Thermo Fisher, P36980). Images were obtained on a Leica SP8 confocal microscope at 20× magnification and analyzed using ImageJ Fiji.

RNA-FISH. RNA-FISH was conducted using the RNAscope Fluorescent Multiplex Reagent kit (ACDBio, 320850) with the ACD HybEZ Hybridization oven according to the manufacturer's instructions. The RNAscope probes used were as follows: Mm-Ifnb1 (406531), Mm-Klrb1c-C2 (424451-C2), Mm-Itgax-C2 (311501-C2), and Mm-Itgam-C3 (311491-C3). Images were obtained using a Leica SP8 confocal microscope at 40× magnification and analyzed using ImageJ Fiji.

In vitro cocultured cells. A sterile coverslip was added to a 24-well plate prior to the seeding of NKT cells and peritoneal macrophages. After performing the desired treatment, the medium was gently removed as to not disturb the coverslip-attached cells. The cells were fixed with 4% PFA for 15 min at 4 °C. Coverslips were briefly rinsed twice with PBS, and the samples were dehydrated using sequential washes of 50% ethanol, 70% ethanol, and 100% ethanol and then rehydrated with PBS. Cells were then treated with 1:15 diluted protease III at room temperature for 30 min and then briefly washed twice with PBS. RNAscope probes were next added to the coverslip and hybridized at 40 °C in the HybEZ Hybridization oven. Each channel was then labeled with the RNAscope Fluorescent Multiplex Reagent kit according to the manufacturer's instructions.

Tumor slides. 10 μm fresh-frozen tumor slices were used for RNA-FISH. Similar to the cultured cells, tumor slices were fixed with 4% PFA at 4 °C for 15 min and followed by serial ethanol treatments. Prior to the protease pretreatment, a hydrophobic barrier was drawn around the tumor slice. Here, undiluted protease IV was used to pretreat the tumor slices. Following the pretreatment, the RNAscope probe hybridization was done as previously stated.

Flow Cytometry. Freshly dissected tumors were digested with 0.2 mg/mL Collagenase P (Roche, 11213857001), 0.2 mg/mL Dispase (Gibco, 17105041), and 0.1 mg/mL DNase I (Roche, 10104159001) in RPMI-1640 containing 2% FBS as described previously (79), with the following modifications. The digestion time was decreased to 20 min twice. Single cell suspension was blocked with rat anti-mouse CD16/CD32 antibody (BioLegend, 101302) in Flow Cytometry Staining buffer (Thermo Fisher, 00-4222-26) for 15 min at 4 °C. Cells were then stained with fluorochrome conjugated antibodies or CD1d-tetramers (*SI Appendix*, Table S1) at 4 °C for 30 min in Flow Cytometry Staining buffer. After staining, the cells were washed twice with Flow Cytometry Staining buffer. Dead cells were identified using DAPI (Thermo, R37606) when it was compatible. All staining and washing were done in a 96-well U-bottom plate with a foil wrapped cover. 1×10^5 singlets were initially collected for each sample in wild type and $CD1d^{-/-}$ mice, and 3×10^5 singlets were collected for each sample in $IFNARI^{-/-}$ mice. 1×10^5 singlets were initially collected for each cultured sample. Cell counts shown were normalized by singlets. Flow cytometry data were obtained using a BD LSRFortessa™ Cell Analyzer and BD Diva software 6.0. Data analysis was done using FlowJo v10 software.

qPCR. Tumor samples were snap frozen in liquid nitrogen and total RNA was isolated using the RNeasy mini kit (Qiagen, 74106), according to the manufacturer's instructions. cDNA was prepared using oligo d(T) primers with the Taqman Reverse Transcription Kit (Thermo, N8080234). Taqman probes for mouse *Tbp* (Mm00446973_m1), *Ifnb1* (Mm00439552_s1), *Mx1* (Mm00487796_m1), *Oas2* (Mm00439552_s1), *Cd3e* (Mm00439552_s1), and *Ifng* (Mm00439552_s1) were used. qPCR was conducted using the Taqman Universal Master Mix II (Thermo, 4440040) on the QuantStudio™ 6 Flex Real-Time PCR System (Thermo Fisher). *Tbp* was used as the endogenous control.

Mouse Hepatic NKT Cell Isolation. Mouse NKT cells were isolated from the liver of C57BL/6J mice. Hepatic lymphocytes were enriched via a 37.5% Percoll centrifugation as described previously (80). Briefly, mouse livers were perfused with Hank's buffer (8.0 g/L NaCl, 0.4 g/L KCl, 3.57 g/L Hepes, 0.06 g/L $Na_2HPO_4 \bullet 2H_2O$, 0.06 g/L KH_2PO_4, pH 7,4) to remove blood cells and the livers were then homogenized in RPMI-1640 (Corning, 10-041-CV) by passing the cells through a 70 μm cell strainer (Corning, 352350). Large debris was removed by centrifugation at 60 g, at 4 °C for 4 min. Cells were then pelleted at 600 g, at 4 °C for 8 min, and resuspended in 10 mL of 37.5% Percoll. Lymphocytes were enriched by centrifugation at 850 g, at 4 °C for 30 min, using a descending rate of four. Red blood cells were next lysed with ACK lysis buffer. The hepatic lymphocytes were then resuspended in complete RPMI-1640 medium (containing 10% FBS, 1% Penicillin-Streptomycin, 50 μM β-mercaptoethanol) and counted. Next, NKT cells were negatively selected by using biotin-labeled antibodies and anti-biotin magnetic beads. 2×10^7 hepatic lymphocytes were centrifuged at 450 g, at 4 °C for 5 min, and resuspended in 500 μL MACS buffer (0.5% BSA, 2 mM EDTA in PBS) containing biotinylated anti-mouse CD8, CD19, CD11b, CD11c, Gr1, TCRγδ, TER-119, CD62L, CD24, and CD49b, and FcR blocking antibodies (*SI Appendix*, Table S2). After 10-min incubation at 4 °C, cells were washed with MACS buffer twice and resuspended in 160 μL MACS buffer. 40 μL of anti-Biotin MicroBeads Ultrapure (Miltenyi Biotec, 130-105-637) was incubated with the biotinylated antibody labeled cells at 4 °C for 15 min. After two washes with MACS buffer, cells were resuspended in 400 μL MACS buffer and loaded into a LS column (Miltenyi Biotec, 130-042-401) for negative selection according to the manufacturer's instructions. The percentage of NKT cells in the flow-out collection was determined by flow cytometry using CD1d-PBS57 tetramer staining.

Mouse Peritoneal Macrophage Isolation. Mouse peritoneal macrophages were collected by rinsing the abdominal cavity of C57BL/6J mice with complete RPMI-1640 medium (containing 10% FBS, 1% Penicillin-Streptomycin, 50 μM β-mercaptoethanol). Red blood cells were lysed with AKC lysis buffer.

NKT Cells and Peritoneal Macrophage Coculture Experiment. 1×10^5/well purified NKT cells were cultured with or without 2×10^5/well peritoneal macrophages in 96-well U-bottomed plates in complete RPMI-1640, and treated with or without 50 ng/mL α-GalCer (KRN700, Avanti Polar Lipids, 867000) for 48 h. For blocking assays, 200 μg/mL of anti-CD40L (Bio X Cell, BE0017), or IgG control (Bio X Cell, BE0091) was added to the culture media. IFNβ in the supernatants was quantified using an ELISA kit to IFNβ (R&D system, DY8234).

NKT Cells and BMDCs Coculture Experiment. BMDCs were generated by 9 d culture of bone marrow cells in complete RPMI-1640 medium supplied with 200 ng/mL recombinant mouse Flt3T (Biolegend, 550704) (81). Media were refreshed every 3 d during the induction of BMDCs. 2×10^5/well purified NKT cells and 4×10^5/well BMDCs were cocultured in 48-well plate and stimulated with α-GalCer (200 ng/mL, Macklin, G862163) for 48 h before adding Brefeldin A (10 μg/mL, MCE, HY-16592) for an additional 12 h of incubation. Cells were subsequently stained with surface markers: CD1d-PBS57-APC tetramer, anti-SiglecH-PacBlue, anti-CD11b-BV650, anti-CD11c-PE/Cy5, anti-CD8a-APC/Cy7, anti-CD40-AF488, anti-TCRβ-BV786, and FcR blocking antibodies (*SI Appendix*, Table S1), followed by intracellular staining with anti-IFNβ (Biolegend, 519202, Clone Poly5192) and subsequent donkey anti-goat-Alexa Fluor 546 (Invitrogen, A11056, 1:500) antibodies by using

Foxp3/Transcription Factor Staining Buffer Set (ebioscience, 00-5523-00). Cells were stored in 1% PFA until analysis.

GSEA. GSEA for our previously published RNAseq data (54) (accession No. GSE193027) was performed by using a preranked list of genes. Briefly, the preranked list based on differential expression was analyzed using GSEA v4.2.3 (Broad Institute, Inc.). Hallmark gene sets were used as the reference gene sets for enrichment. Gene set enrichment plots were obtained from the GSEA v4.2.3, and the ranked enrichment gene sets were plotted using Prism 9.0 (GraphPad Software) based on the FDR and the NES values obtained from GSEA software.

RNA Sequencing and Data Analysis. RNA integrity number (RIN) was determined using the 2100 Bioanalyzer System (Agilent Technologies) with the Agilent RNA 6000 Nano Kit (Agilent Technologies, 5067-1511). Only RNA with a RIN > 8 was used for sequencing library preparation. Briefly, 4 μg of tumor-derived RNA from each sample was used for library preparation, which was assembled using the TruSeq Stranded Total RNA kit (Illumina, 20020596) according to the manufacturer's instructions, except for the modification of 12 PCR cycles instead of the recommended 15. Single End 76 base pair sequencing was done at the CSHL Next Generation Sequencing Core facility on the NextSeq High Output platform. RNAseq data were analyzed by the CSHL Bioinformatics Core facility. In general, FastQC, STAR, featurecounts, RSEM, and GSEA were used for data analysis with the standard setting.

RNAseq data from our previous published work (54) (accession No. GSE193027) were used in heat map to depict the differentially expressed genes comparing subcutaneous sgKRT19-edited tumors and sgScramble control tumors. Genes that changed more than twofold and had an adjusted *P*-value less than 0.0001 were depicted in the heat map by showing the normalized expression z-score of each gene in individual tumors.

Statistical Analysis. Unless indicated, all results are presented as the means ± SEMs. The statistical analysis was described in the figure legends. All statistical analyses were performed using GraphPad Prism Software version 9.1.0, using a *P* value of $P < 0.05$ to denote statistical significance. The individual *P* values are denoted as $*P < 0.05$, $**P < 0.01$, $***P < 0.001$, $****P < 0.0001$.

Data, Materials, and Software Availability. RNAseq data for Fig. 5*C* is available in the Gene Expression Omnibus database (accession no. GSE270858) (82). Previously published data were used for this work (accession no. GSE193027) (83). All other study data are included in the manuscript and/or *SI Appendix*.

ACKNOWLEDGMENTS. We thank Dr. David Tuveson at CSHL for providing KPC1242 mouse pancreatic cancer cell line. We thank Dr. Yongjun Qian, Dr. Xueyan He, and Dr. Min Yao at CSHL for reading and commenting on the draft. This work was performed in the CSHL facilities of Animal, DNA Sequencing, Flow Cytometry, Histology and Microscopy which are supported in part by the Cancer Center Support Grant 5P30CA045508. This work was supported by the Lustgarten Foundation (D.T.F.), the Thompson Family Foundation (D.T.F.), the Cedar Hill Foundation (D.T.F.), the Simons Foundation (D.T.F.), the Sponsored Research Agreement with Mestag Therapeutics Ltd. (J.L., P.M., and D.T.F.), NIH T32 Training Grant T32GM008444 (P.M.), and the NIH NCI F30 Ruth L. Kirschstein National Research Service Award (P.M.).

1. R. L. Siegel, A. N. Giaquinto, A. Jemal, Cancer statistics, 2024. *CA Cancer J. Clin.* **74**, 12–49 (2024).
2. W. Park, A. Chawla, E. M. O'Reilly, Pancreatic cancer. *JAMA* **326**, 851–862 (2021).
3. J. R. Brahmer *et al.*, Safety and activity of anti–PD-L1 antibody in patients with advanced cancer. *N. Engl. J. Med.* **366**, 2455–2465 (2012).
4. S. L. Topalian *et al.*, Safety, activity, and immune correlates of anti–PD-1 antibody in cancer. *N. Engl. J. Med.* **366**, 2443–2454 (2012).
5. R. E. Royal *et al.*, Phase 2 trial of single agent Ipilimumab (anti-CTLA-4) for locally advanced or metastatic pancreatic adenocarcinoma. *J. Immunother.* **33**, 828–833 (2010).
6. W. J. Ho, E. M. Jaffee, L. Zheng, The tumour microenvironment in pancreatic cancer–clinical challenges and opportunities. *Nat. Rev. Clin. Oncol.* **17**, 527–540 (2020).
7. G. L. Beatty *et al.*, CD40 agonists alter tumor stroma and show efficacy against pancreatic carcinoma in mice and humans. *Science* **331**, 1612–1616 (2011).
8. Y. D. Seo *et al.*, Mobilization of CD8(+) T cells via CXCR4 blockade facilitates PD-1 checkpoint therapy in human pancreatic cancer. *Clin. Cancer Res.* **25**, 3934–3945 (2019).
9. D. Biasci *et al.*, CXCR4 inhibition in human pancreatic and colorectal cancers induces an integrated immune response. *Proc. Natl. Acad. Sci. U.S.A.* **117**, 28960–28970 (2020).
10. B. Bockorny *et al.*, BL-8040, a CXCR4 antagonist, in combination with pembrolizumab and chemotherapy for pancreatic cancer: The COMBAT trial. *Nat. Med.* **26**, 878–885 (2020).
11. K. T. Byrne *et al.*, Neoadjuvant selicrelumab, an agonist CD40 antibody, induces changes in the tumor microenvironment in patients with resectable pancreatic cancer. *Clin. Cancer Res.* **27**, 4574–4586 (2021).
12. H. Jiang *et al.*, Targeting focal adhesion kinase renders pancreatic cancers responsive to checkpoint immunotherapy. *Nat. Med.* **22**, 851–860 (2016).
13. E. P. Vonderhaar *et al.*, STING activated tumor-intrinsic type I interferon signaling promotes CXCR3 dependent antitumor immunity in pancreatic cancer. *Cell. Mol. Gastroenterol. Hepatol.* **12**, 41–58 (2021).
14. L. Zitvogel, L. Galluzzi, O. Kepp, M. J. Smyth, G. Kroemer, Type I interferons in anticancer immunity. *Nat. Rev. Immunol.* **15**, 405–414 (2015).
15. R. Yu, B. Zhu, D. Chen, Type I interferon-mediated tumor immunity and its role in immunotherapy. *Cell. Mol. Life Sci.* **79**, 191 (2022).
16. G. P. Dunn *et al.*, A critical function for type I interferons in cancer immunoediting. *Nat. Immunol.* **6**, 722–729 (2005).
17. M. S. Diamond *et al.*, Type I interferon is selectively required by dendritic cells for immune rejection of tumors. *J. Exp. Med.* **208**, 1989–2003 (2011).
18. M. B. Fuertes *et al.*, Host type I IFN signals are required for antitumor CD8+ T cell responses through CD8α+ dendritic cells. *J. Exp. Med.* **208**, 2005–2016 (2011).
19. J. B. Swann *et al.*, Type I IFN contributes to NK cell homeostasis, activation, and antitumor function. *J. Immunol.* **178**, 7540–7549 (2007).
20. C. Feig *et al.*, Targeting CXCL12 from FAP-expressing carcinoma-associated fibroblasts synergizes with anti–PD-L1 immunotherapy in pancreatic cancer. *Proc. Natl. Acad. Sci. U.S.A.* **110**, 20212–20217 (2013).
21. I. M. Stromnes *et al.*, Targeted depletion of an MDSC subset unmasks pancreatic ductal adenocarcinoma to adaptive immunity. *Gut* **63**, 1769–1781 (2014).
22. S. Hegde *et al.*, Dendritic cell paucity leads to dysfunctional immune surveillance in pancreatic cancer. *Cancer cell* **37**, 289–307.e9 (2020).
23. J. Li *et al.*, Tumor cell-intrinsic factors underlie heterogeneity of immune cell infiltration and response to immunotherapy. *Immunity* **49**, 178–193.e7 (2018).
24. R. Z. Panni *et al.*, Agonism of CD11b reprograms innate immunity to sensitize pancreatic cancer to immunotherapies. *Sci. Transl. Med.* **11**, eaau9240 (2019).
25. M. Davis *et al.*, Effect of pemetrexed on innate immune killer cells and adaptive immune T cells in subjects with adenocarcinoma of the pancreas. *J. Immunother.* **35**, 629–640 (2012).
26. E. Gürlevik *et al.*, Administration of gemcitabine after pancreatic tumor resection in mice induces an antitumor immune response mediated by natural killer cells. *Gastroenterology* **151**, 338–350.e7 (2016).
27. D. I. Godfrey, H. R. MacDonald, M. Kronenberg, M. J. Smyth, L. Van Kaer, NKT cells: What's in a name? *Nat. Rev. Immunol.* **4**, 231–237 (2004).
28. A. Bendelac, P. B. Savage, L. Teyton, The biology of NKT cells. *Ann. Rev. Immunol.* **25**, 297–336 (2007).
29. P. J. Brennan, M. Brigl, M. B. Brenner, Invariant natural killer T cells: An innate activation scheme linked to diverse effector functions. *Nat. Rev. Immunol.* **13**, 101–117 (2013).
30. N. Y. Crowe, M. J. Smyth, D. I. Godfrey, A critical role for natural killer T cells in immunosurveillance of methylcholanthrene-induced sarcomas. *J. Exp. Med.* **196**, 119–127 (2002).
31. N. Y. Crowe *et al.*, Differential antitumor immunity mediated by NKT cell subsets in vivo. *J. Exp. Med.* **202**, 1279–1288 (2005).
32. G. J. Renukaradhya *et al.*, Type I NKT cells protect (and type II NKT cells suppress) the host's innate antitumor immune response to a B-cell lymphoma. *Blood* **111**, 5637–5645 (2008).
33. M. Terabe, J. A. Berzofsky, The role of NKT cells in tumor immunity. *Adv. Cancer Res.* **101**, 277–348 (2008).
34. J. B. Swann *et al.*, Type I natural killer T cells suppress tumors caused by p53 loss in mice. *Blood* **113**, 6382–6385 (2009).
35. H. Bassiri *et al.*, iNKT cell cytotoxic responses control T-lymphoma growth in vitro and in vivo. *Cancer Immunol. Res.* **2**, 59–69 (2014).
36. F. C. Robertson, J. A. Berzofsky, M. Terabe, NKT cell networks in the regulation of tumor immunity. *Front. Immunol.* **5**, 1–12 (2014).
37. R. M. McEwen-Smith, M. Salio, V. Cerundolo, The regulatory role of invariant NKT cells in tumor immunity. *Cancer Immunol. Res.* **3**, 425–435 (2015).
38. M. Terabe, J. A. Berzofsky, Tissue-specific roles of NKT cells in tumor immunity. *Front. Immunol.* **9**, 1838 (2018).
39. C. Ma *et al.*, Gut microbiome-mediated bile acid metabolism regulates liver cancer via NKT cells. *Science* **360**, eaan5931 (2018).
40. F. Cortesi *et al.*, Bimodal CD40/Fas-dependent crosstalk between iNKT cells and tumor-associated macrophages impairs prostate cancer progression. *Cell Rep.* **22**, 3006–3020 (2018).
41. G. Cui *et al.*, A circulating subset of iNKT cells mediates antitumor and antiviral immunity. *Sci. Immunol.* **7**, eabj8760 (2022).
42. J. Burks, P. B. Olkhanud, J. A. Berzofsky, The role of NKT cells in gastrointestinal cancers. *Oncoimmunology* **11**, 2009666 (2022).
43. M. Brigl, L. Bry, S. C. Kent, J. E. Gumperz, M. B. Brenner, Mechanism of CD1d-restricted natural killer T cell activation during microbial infection. *Nat. Immunol.* **4**, 1230–1237 (2003).
44. J. Mattner *et al.*, Exogenous and endogenous glycolipid antigens activate NKT cells during microbial infections. *Nature* **434**, 525–529 (2005).
45. J. Rossjohn, D. G. Pellicci, O. Patel, L. Gapin, D. I. Godfrey, Recognition of CD1d-restricted antigens by natural killer T cells. *Nat. Rev. Immunol.* **12**, 845–857 (2012).
46. C. Carnaud *et al.*, Cutting edge: Cross-talk between cells of the innate immune system: NKT cells rapidly activate NK cells. *J. Immunol.* **163**, 4647–4650 (1999).
47. H. Kitamura *et al.*, The natural killer T (NKT) cell ligand alpha-galactosylceramide demonstrates its immunopotentiating effect by inducing interleukin (IL)-12 production by dendritic cells and IL-12 receptor expression on NKT cells. *J. Exp. Med.* **189**, 1121–1128 (1999).
48. M. Tomura *et al.*, A novel function of Vα14+CD4+NKT cells: Stimulation of IL-12 production by antigen-presenting cells in the innate immune system. *J. Immunol.* **163**, 93–101 (1999).
49. G. Eberl, H. R. MacDonald, Selective induction of NK cell proliferation and cytotoxicity by activated NKT cells. *Eur. J. Immunol.* **30**, 985–992 (2000).
50. S. Fujii, K. Shimizu, C. Smith, L. Bonifaz, R. M. Steinman, Activation of natural killer T cells by alpha-galactosylceramide rapidly induces the full maturation of dendritic cells in vivo and thereby acts as an adjuvant for combined CD4 and CD8 T cell immunity to a coadministered protein. *J. Exp. Med.* **198**, 267–279 (2003).

51. S. Fujii, K. Liu, C. Smith, A. J. Bonito, R. M. Steinman, The linkage of innate to adaptive immunity via maturing dendritic cells in vivo requires CD40 ligation in addition to antigen presentation and CD80/86 costimulation. *J. Exp. Med.* **199**, 1607–1618 (2004).
52. C. De Santo *et al.*, Invariant NKT cells reduce the immunosuppressive activity of influenza A virus-induced myeloid-derived suppressor cells in mice and humans. *J. Clin. Invest.* **118**, 4036–4048 (2008).
53. J. A. Greene, J. L. DeVecchio, M. P. Gould, J. J. Auletta, F. P. Heinzel, In vivo and in vitro regulation of type I IFN synthesis by synergistic effects of CD40 and type II IFN. *J. Immunol.* **176**, 5995–6003 (2006).
54. Z. Wang *et al.*, Carcinomas assemble a filamentous CXCL12–keratin-19 coating that suppresses T cell–mediated immune attack. *Proc. Natl. Acad. Sci. U.S.A.* **119**, e2119463119 (2022).
55. S. R. Woo *et al.*, STING-dependent cytosolic DNA sensing mediates innate immune recognition of immunogenic tumors. *Immunity* **41**, 830–842 (2014).
56. L. Deng *et al.*, STING-dependent cytosolic DNA sensing promotes radiation-induced type I interferon-dependent antitumor immunity in immunogenic tumors. *Immunity* **41**, 843–852 (2014).
57. M. Bedard *et al.*, Sterile activation of invariant natural killer T cells by ER-stressed antigen-presenting cells. *Proc. Natl. Acad. Sci. U.S.A.* **116**, 23671–23681 (2019).
58. T. Olszak *et al.*, Microbial exposure during early life has persistent effects on natural killer T cell function. *Science* **336**, 489–493 (2012).
59. N. B. Janakiram *et al.*, Loss of natural killer T cells promotes pancreatic cancer in LSL-Kras(G12D/+) mice. *Immunology* **152**, 36–51 (2017).
60. S. Nagaraj *et al.*, Dendritic cells pulsed with alpha-galactosylceramide induce anti-tumor immunity against pancreatic cancer in vivo. *Int. Immunol.* **18**, 1279–1283 (2006).
61. A. Nelson, S. Gebremeskel, B. D. Lichty, B. Johnston, Natural killer T cell immunotherapy combined with IL-15-expressing oncolytic virotherapy and PD-1 blockade mediates pancreatic tumor regression. *J. Immunother. Cancer* **10**, e003923 (2022).
62. M. S. Diamond *et al.*, Type I interferon is selectively required by dendritic cells for immune rejection of tumors. *J. Exp. Med.* **208**, 1989–2003 (2011).
63. M. B. Fuertes *et al.*, Host type I IFN signals are required for antitumor CD8+ T cell responses through CD8alpha+ dendritic cells. *J. Exp. Med.* **208**, 2005–2016 (2011).
64. B. Guillot *et al.*, The expression of cytotoxic mediators is altered in mononuclear cells of patients with melanoma and increased by interferon-alpha treatment. *Br. J. Dermatol.* **152**, 690–696 (2005).
65. A. Marcus *et al.*, Tumor-derived cGAMP triggers a STING-mediated interferon response in non-tumor cells to activate the NK cell response. *Immunity* **49**, 754–763.e4 (2018).
66. C. Zoglmeier *et al.*, CpG blocks immunosuppression by myeloid-derived suppressor cells in tumor-bearing mice. *Clin. Cancer Res.* **17**, 1765–1775 (2011).
67. A. Sistigu *et al.*, Cancer cell-autonomous contribution of type I interferon signaling to the efficacy of chemotherapy. *Nat. Med.* **20**, 1301–1309 (2014).
68. M. E. Mikucki *et al.*, Non-redundant requirement for CXCR3 signalling during tumoricidal T-cell trafficking across tumour vascular checkpoints. *Nat. Commun.* **6**, 7458 (2015).
69. K. Kohli, V. G. Pillarisetty, T. S. Kim, Key chemokines direct migration of immune cells in solid tumors. *Cancer Gene Ther.* **29**, 10–21 (2022).
70. P. M. Brailey *et al.*, CD1d-dependent rewiring of lipid metabolism in macrophages regulates innate immune responses. *Nat. Commun.* **13**, 6723 (2022).
71. S. Cui *et al.*, CD1d1 intrinsic signaling in macrophages controls NLRP3 inflammasome expression during inflammation. *Sci. Adv.* **6**, eaaz7290 (2020).
72. A. Nelson, J. D. Lukacs, B. Johnston, The current landscape of NKT cell immunotherapy and the hills ahead. *Cancers (Basel)* **13**, 5174 (2021).
73. K. Yamasaki *et al.*, Induction of NKT cell-specific immune responses in cancer tissues after NKT cell-targeted adoptive immunotherapy. *Clin. Immunol.* **138**, 255–265 (2011).
74. A. Rotolo *et al.*, Enhanced anti-lymphoma activity of CAR19-iNKT cells underpinned by dual CD19 and CD1d targeting. *Cancer Cell* **34**, 596–610.e11 (2018).
75. A. Heczey *et al.*, Anti-GD2 CAR-NKT cells in patients with relapsed or refractory neuroblastoma: An interim analysis. *Nat. Med.* **26**, 1686–1690 (2020).
76. T. Toyoda *et al.*, Phase II study of α-galactosylceramide–pulsed antigen-presenting cells in patients with advanced or recurrent non-small cell lung cancer. *J. Immunother. Cancer* **8**, e000316 (2020).
77. B. Bockorny *et al.*, Motixafortide and pembrolizumab combined to nanoliposomal irinotecan, fluorouracil, and folinic acid in metastatic pancreatic cancer: The COMBAT/ KEYNOTE-202 trial. *Clin. Cancer Res.* **27**, 5020–5027 (2021).
78. Y. Y. Janjigian *et al.*, First-line nivolumab plus chemotherapy versus chemotherapy alone for advanced gastric, gastro-oesophageal junction, and oesophageal adenocarcinoma (CheckMate 649): A randomised, open-label, phase 3 trial. *Lancet* **398**, 27–40 (2021).
79. R. Yan, P. Moresco, B. Gegenhuber, D. T. Fearon, T cell–mediated development of stromal fibroblasts with an immune-enhancing chemokine profile. *Cancer Immunol. Res.* **11**, 1044–1054 (2023).
80. Á. de Mingo Pulido *et al.*, Differential role of cathepsins S and B in hepatic APC-mediated NKT cell activation and cytokine secretion. *Front. Immunol.* **9**, 1–14 (2018).
81. S. H. Naik *et al.*, Cutting edge: Generation of splenic CD8+ and CD8− dendritic cell equivalents in Fms-like tyrosine kinase 3 ligand bone marrow cultures. *J. Immunol.* **174**, 6592–6597 (2005).
82. J. Li, D. T. Fearon, Data from "Intratumoral NKT cell accumulation promotes antitumor immunity in pancreatic cancer." GEO. https://www.ncbi.nlm.nih.gov/geo/query/acc.cgi?acc=GSE270858. Deposited 26 June 2024.
83. Z. Wang, D. T. Fearon, Data from "The immunological comparison of control PDA tumors and Krt19-edited PDA tumors." GEO. https://www.ncbi.nlm.nih.gov/geo/query/acc.cgi?acc=GSE193027. Deposited 4 January 2022.